Chapter 11
Mechanical-Chemical (MC) Processes

Norihiro Watanabe, Renchao Lu, Joshua Taron, Wenkui He, Eunseon Jang and Haibing Shao

11.1 Permeability Evolution of a Quartz Fracture Due to Free-Face Dissolution and Pressure Solution

Norihiro Watanabe and Joshua Taron

This benchmark focuses on permeability evolution of a quartz fracture due to water-rock interaction under confining pressure. Free-face mineral dissolution/precipitation at pore walls and pressure solution (i.e. stress enhanced dissolution) at asperity contacts are assumed as dominant mechanisms to alter the fracture void space geometry and its permeability. Effects of a rock matrix on flow and solute transport are ignored in the current model.

11.1.1 Theory

We consider a quartz fracture having upper and lower surfaces in contact. In a macroscopic view, the fracture can be statistically represented using the mean mechanical aperture b_m [m] and the contact area ratio R_c [-]. Corresponding to water flow through the fracture, the fracture void space geometry can be altered by the following water-

N. Watanabe (✉) · R. Lu (✉) · W. He · E. Jang · H.B. Shao
Helmholtz Centre for Environmental Research—UFZ, Leipzig, Germany
e-mail: norihiro.watanabe@ufz.de

J. Taron
U.S. Geological Survey, Menlo Park, CA, USA

R. Lu · W. He · E. Jang
Technische Universität Dresden, Dresden, Germany
e-mail: renchao.lu@ufz.de

H.B. Shao
Technische Universität Bergakademie Freiberg, Freiberg, Germany

O. Kolditz et al. (eds.), *Thermo-Hydro-Mechanical-Chemical Processes in Fractured Porous Media: Modelling and Benchmarking*, Terrestrial Environmental Sciences, DOI 10.1007/978-3-319-29224-3_11

quartz interaction at the fracture surfaces:

$$SiO_2 + 2H_2O \leftrightarrow H_4SiO_4(aq) \tag{11.1.1}$$

Since the fracture is under confining stress, the reaction rate will be different at hydrostatically stressed pore walls and at non-hydrostatically stressed asperity contacts. At the pore-walls, the reaction is free-face quartz dissolution and precipitation as

$$\dot{m}_p = 2(1 - R_c)k^+\left(1 - \frac{C_p}{C^h_{eq}}\right). \tag{11.1.2}$$

with the free-face dissolution rate m_p [mol/m^2/s], the dissolution rate constant k^+ [mol/m^2/s], solute concentration in the pore space C_p [mol/m^3], and the solubility under hydrostatic pressure C^h_{eq} [mol/m^3]. At fracture asperity contacts, pressure solution process can be dominant. Following a pressure solution model for intergranular contacts in Taron and Elsworth (2010a, b), the stress-enhanced reaction rate m_i can be expressed as

$$\dot{m}_i = 2\alpha R_c a^\sigma k^+\left(1 - \frac{C_i}{a^\sigma C^h_{eq}}\right) \tag{11.1.3}$$

with the intergranular roughness α, the activity of solid silica under stress a^σ, and the intergranular concentration C_i [mol/m^3]. The activity of stressed solid silica is given as

$$a^\sigma = \exp\left(\frac{\max(\sigma_a - \sigma_c\beta_c^2, 0)}{\alpha RT}V_m\right). \tag{11.1.4}$$

where σ_a is the contact stress [Pa], σ_c is the critical stress [Pa], β_c is the burial constant, R is the gas constant [J/K/mol], T is temperature [K], V_m is the molar volume [m^3/mol]. If the contact stress is below the critical threshold $\sigma_c\beta_c^2$, the activity becomes unity and no enhancement is applied to the intergranular reaction.

Including the above reaction rates and solute exchange between the pore space and the intergranular zones, solute mass balances in a fracture void space and intergranular zones can be given as

$$b_m\frac{\partial C_p}{\partial t} + \nabla \times b_m\left(-\mathbf{D}'\nabla C_p + \mathbf{q}C_p\right) = 2(1 - R_c)k^+\left(1 - \frac{C_p}{C^h_{eq}}\right) + 8R_cD_f\omega(C_i - C_p) \tag{11.1.5}$$

$$\omega R_c\frac{dC_i}{dt} = 2\alpha R_c a^\sigma k^+\left(1 - \frac{C_i}{a^\sigma C^h_{eq}}\right) - 8R_cD_f\omega(C_i - C_p), \tag{11.1.6}$$

with the dispersion tensor $\mathbf{D}'$ [m^2/s], the flow velocity $\mathbf{q}$ [m/s], the intergranular water film thickness ω [m], and the intergranular molecular diffusivity D_f [m^2/s]. The dispersion tensor is given as

$$D'_{ij} = D_m \delta_{ij} + \alpha_T |\mathbf{v}| \delta_{ij} + (\alpha_L - \alpha_T) \frac{v_i v_j}{|\mathbf{v}|} \tag{11.1.7}$$

with the molecular diffusivity D_m [m^2/s], the longitudinal and transversal dispersion coefficients α_L, α_T [m]. The intergranular molecular diffusivity can be estimated by the Stokes-Einstein equation (Renard et al. 1999).

Fracture void space will be altered as a result of the free-face reaction and pressure solution at asperity contacts. Total aperture change can be estimated as a linear combination of the above effects

$$\Delta b_m = \frac{\Delta m_p V_m}{A_p} - \frac{\Delta m_i V_m}{A_i} \tag{11.1.8}$$

where A_p and A_i are the surface area of pore walls and intergranular zones, respectively. As it is clear from the equation, the free-face dissolution tries to increase the aperture while the pressure solution has the opposite influence. Contact area ratio will also be updated corresponding to the aperture changes.

The void space geometry has an significant impact on the fracture permeability. In the case of laminar flow without gravitational effects, groundwater flow through the fracture can be expressed as

$$b_m S_s \frac{\partial p}{\partial t} + \nabla \times b_h (-\frac{k}{\mu} \nabla p) = 0 \tag{11.1.9}$$

where b_h denote the hydraulic aperture [m], S_s is the specific storage [1/Pa], p is water pressure [Pa], k is the fracture permeability [m^2], and μ is the fluid dynamic viscosity [Pa s]. The fracture permeability is given from the cubic law (Snow 1969)

$$k = \frac{b_h^2}{12}, \tag{11.1.10}$$

and the hydraulic aperture can be estimated from the mean mechanical aperture and the contact area ratio as Walsh (1981)

$$b_h^3 = \frac{1 - R_c}{1 + R_c} b_m^3. \tag{11.1.11}$$

11.1.2 Example

This example simulates a flow-through experiment of a novaculite fracture under confining pressure reported in Yasuhara et al. (2006). In particular, we focus on the experiment result until 1292 h when a monotonic decrease of the fracture permeability was observed. The experimental fracture has a length of 89.5 mm and a width of 50 mm. Its initial hydraulic aperture was estimated as 18.5 μm from the cubic law. The fracture is under confining pressure of 1.38 MPa. Deionized water at 20 °C is injected with time-dependent flow rates (Table 11.1) and the outlet pressure is fixed to 345 kPa.

Table 11.1 Time dependent boundary conditions

t [h]	T [°C]	Q_{in} [mL/min]	p_{out} [kPa]	C_{in} [ppm]
0–121	20	1.0	345	0
121–380	20	0.5	345	0
380–858	20	0.25	345	0
858–930	20	0	–	–
930–1266	20	0.25	345	0
1266–1292	20	0.125	345	0

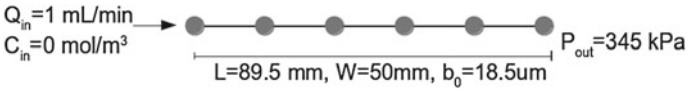

Fig. 11.1 1D fracture model

In this example, we simplify the fracture geometry as a 1D homogenized model along a flow path (Fig. 11.1). The contact area ratio can be calculated from the mean aperture using the aperture–contact area ratio relationship given in Yasuhara et al. (2006).

$$b_m = 2.5 \times 10^{-6} + 16.0 \times 10^{-6} \exp\left(-\frac{R_c - 5}{20}\right). \tag{11.1.12}$$

Using the relationship and the Walsh's hydraulic aperture model, the initial mean aperture and contact area ratio can be calculated as 19.04 μm and 4.3 %, respectively. For quartz dissolution, we take the dissolution rate constant from Rimstidt (1997); Rimstidt and Barnes (1980)

$$\log_{10} k^+ = -0.7324 - 3705.12/T \tag{11.1.13}$$

and solubility [mol/kg-w] from Rimstidt (1997)

$$\log_{10} m = -0.0254 - 1107.12/T. \tag{11.1.14}$$

Reactive surface area is assumed to be equal to the geometric fracture surface area. Because of limited data availability, there is considerable uncertainty in the geochemical parameters in the experimented system. To match the simulation result with the experiment, the dissolution rate had to be enhanced by a factor of 7×10^5. All the other material parameters are listed in Table 11.2.

Numerical solution of the problem can be obtained by using the finite element method to both the flow and transport equations. The numerical model employs a mesh with linear line elements having a length of 1.1 mm and the implicit backward Euler method with an adaptive time stepping.

Table 11.2 Model parameters at $T = 20\,°C$

Parameter	Value
Quartz dissolution rate constant	4.25×10^{-14} mol/m^2/s
Quartz solubility	4.4 ppm
Dissolution rate enhancement	7×10^5
Water density	998.3 kg/m^3
Water dynamic viscosity	0.001 Pa s
Molecular diffusion coefficient	10^{-9} m^2/s
Specific storage	4.6×10^{-10} 1/Pa
Initial mean aperture	19.04 μm
Initial contact ratio	4.3 %
Intergranular thickness	4 nm
Intergranular roughness	0.3
Intergranular diffusion coefficient	0.43×10^{-9} m^2/s
Burial constant	0.1

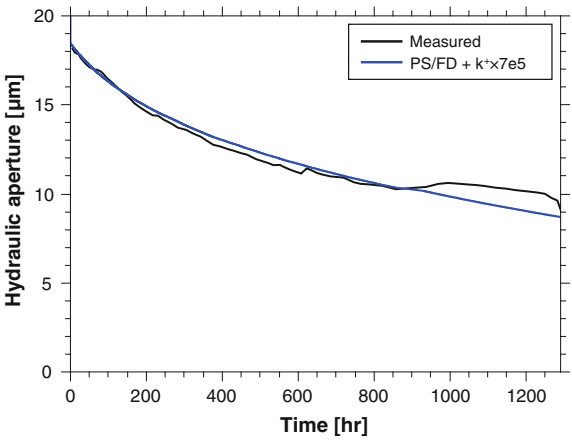

Fig. 11.2 Simulated fracture hydraulic aperture evolution

The simulation result as well as the experimental results are presented in terms of the fracture hydraulic aperture and effluent silica concentrations in Figs. 11.2 and 11.3. The fracture hydraulic aperture was calculated by

$$< b_h >= \sqrt[3]{\frac{12\mu LQ}{W(p_{\text{in}} - p_{\text{out}})}} \tag{11.1.15}$$

with the fracture length L and the width W. Effluent concentrations were taken from concentrations at the outlet (x = L). The simulation reproduces both the monotonic decrease of the fracture permeability and effluent concentrations observed in the experiment.

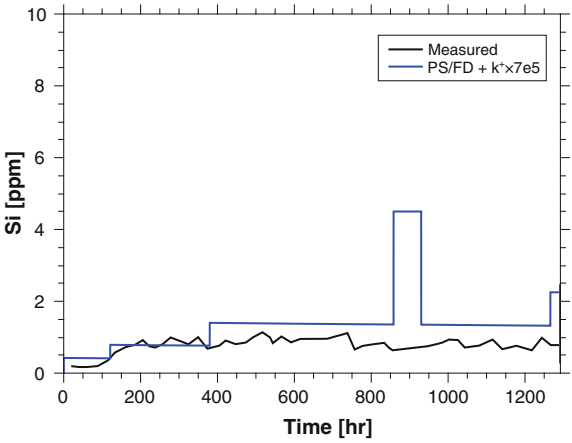

Fig. 11.3 Simulated effluent Si concentrations

11.2 Free-Face Dissolution from Granite Fracture Surfaces

Renchao Lu, Wenkui He, Eunseon Jang, Haibing Shao, Norihiro Watanabe

In this benchmark, we focus on free-face dissolution from granite fracture surfaces when deionized water flows through the fracture surface. Laboratory-scale batch experiments are detailedly presented in Yasuhara et al. (2011). To better understand chemical weathering in a multi-mineral-constituted system with flowing water, a 1D reactive transport model is simulated using OpenGeoSys#IPhreeqc simulator. The simulated results are verified against Phreeqc (Parkhurst et al. 1999).

11.2.1 Theory

Granite is composed of quartz and feldspar (k-feldspar, albite and anorthite) with minor amounts of biotite (annite and phlogopite). When deionized water flows through the fracture surfaces, water-granite interactions will result in continuous mineral dissolution. The involved kinetic reactions and corresponding logarithmic equilibrium constants are listed in Table 11.3.

Dissolution-precipitation rates follow the widely used kinetic rate equation for multiple mechanisms

$$\dot{m} = \sum_i k_i^+ \left(1 - \left(\frac{Q}{K_{eq}}\right)^{p_i}\right)^{q_i}, \tag{11.2.1}$$

where $\dot{m}$ [mol/m^2/s] is the mass removal rate per unit area, k_i^+ [mol/m^2/s] is the dissolution rate constant in the ith mechanism, Q [-] is the activity product, K_{eq} [-] is the equilibrium constant, p_i [-] and q_i [-] are chemical affinity parameters in the ith mechanism.

Table 11.3 Kinetic reactions involved in the water-granite interactions and corresponding logarithmic equilibrium constants

Mineral	Kinetic reactions	$^{a}\log K_{eq}$
Quartz	$SiO_2 + 2H_2O \rightarrow H_4SiO_4(aq)$	−4.00
K-feldspar:	$KAlSi_3O_8 + 4H^+ + 4H_2O \rightarrow Al^{3+} + K^+ + 3H_4SiO_4(aq)$	0.92
Albite	$NaAlSi_3O_8 + 4H^+ + 4H_2O \rightarrow Al^{3+} + Na^+ + 3H_4SiO_4(aq)$	2.76
Anorthite	$CaAl_2(SiO_4)_2 + 8H^+ \rightarrow 2Al^{3+} + Ca^{2+} + 2H_4SiO_4(aq)$	26.58
Annite	$KFe_3AlSi_3O_10(OH)_2 + 10H^+ \rightarrow$ $Al^{3+} + K^+ + 3Fe^{2+} + 3H_4SiO_4(aq)$	29.47
Phlogopite	$KAlMg_3Si_3O_10(OH)_2 + 10H^+ \rightarrow$ $Al^{3+} + K^+ + 3Mg^{2+} + 3H_4SiO_4(aq)$	37.44

$^{a}\log K_{eq}$ is the temperature-dependent logarithmic equilibrium constant. 25 °C is prescribed as reference temperature and given values are extracted from PHREEQC llnl database

The dissolution rate constant k^+ has Arrhenius-type dependence with temperature, and pH value, namely the negative logarithmic form of activity of hydrogen ion a_{H^+}, also has an impact on it which takes the form

$$k^+ = Ae^{-\frac{E}{RT}} a_{H^+}^{n_{H^+}}, \tag{11.2.2}$$

where A [mol/m^2/s] is the Arrhenius pre-exponential factor, E [J/mol] is the Arrhenius activation energy, a_{H^+} [-] is the activity of hydrogen ion, n_{H^+} [-] is the H^+ catalysis constant. Generally, acid mechanism, neutral mechanism and base mechanism are considered.

Introducing roughness factor for minerals as f_r [-], the solute transport equation for a product j produces the relationship

$$b\frac{\partial C_j}{\partial t} + \nabla \times \left(-\mathbf{D}\nabla C_j + b\mathbf{q}C_j\right) = \sum_{m=1}^{n} \phi_m s_{mj} f_{r,m} \dot{m}_m \tag{11.2.3}$$

with the fracture aperture b [m], the dispersion tensor $\mathbf{D}$ [m^2/s], the flow velocity $\mathbf{q}$ [m/s], the surface area ratio for mineral m in a unit area ϕ_m and the stoichiometric coefficient of the product j in the reaction m s_{mj}. The dispersion tensor is given as

$$D_{ij} = bD_m\delta_{ij} + b\alpha_T|\mathbf{v}|\delta_{ij} + b\left(\alpha_L - \alpha_T\right)\frac{v_i v_j}{|\mathbf{v}|} \tag{11.2.4}$$

with the molecular diffusivity D_m [m^2/s], the longitudinal and transveral dispersion coefficients α_L, α_T [m]. The roughness factor for mineral m is

$$f_{r,m} = \frac{S_m d_m \rho_m}{6}, \tag{11.2.5}$$

where S_m [m^2], d_m [m] and ρ_m [kg/m^3] are specific surface area, grain diameter and density of mineral m, respectively.

Table 11.4 Kinetic reactions involved in the water-granite interactions and corresponding logarithmic equilibrium constants

Mineral	Density (kg/m^3) $\times 10^3$	Surface area ratio (%)
Quartz	2.65	50
K-feldspar	2.55	25
Albite	2.62	10
Anorthite	2.75	10
Annite	2.10	5
Phlogopite	2.10	5

In the case of laminar flow without gravitational effects, groundwater flow through the parallel fracture can be expressed as

$$bS_s \frac{\partial p}{\partial t} + \nabla \times b\left(-\frac{k}{\mu}\nabla p\right) = 0 \tag{11.2.6}$$

where S_s [1/Pa] is the specific storage, p [Pa] is water pressure, k [m^2] is the fracture permeability, and μ [Pa s] is the fluid dynamic viscosity. The fracture permeability is given from the cubic law (Snow 1969)

$$k = \frac{b^2}{12} \tag{11.2.7}$$

11.2.2 Problem Definition

Granite samples used for the experiments are collected from a borehole, roughly 200 m in depth, at the construction site of the Mizunami Underground Research Laboratory (MIU) in central Japan. Reactive surface area ratios for minerals at the fracture surface pairings are approximated by counting representative particles in a square-shape thin-section sample with a side length of 2 mm (Table 11.4). The grain diameter and specific surface area are 178 μm and 0.51 m^2/g, respectively, revealed from the BET analysis. The experimental fracture induced by the Brazilian test has a length of 60 mm and a width of 30 mm. In the model, the fracture is approximated as a parallel plate with a uniform aperture, 5.7 μm. The differential pressure between the inlet and outlet is prescribed as 0.04 MPa to drive deionized water flow through the fracture. The experimental temperature is 25 °C. Figure 11.4 is a schematic of the 1D fracture model.

All the reaction parameters are taken from U.S. Geological Survey Open File Report 2004- 1068 as shown in Table 11.5 (Palandri and Kharaka 2004b).

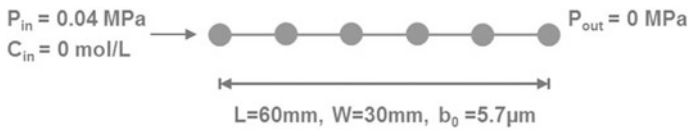

Fig. 11.4 a schmatic of the 1D fracture model

Table 11.5 Parameters used for calculating dissolution rate constants at given temperature and pH value

Mineral	Acid			Neutral		Base		
	log k_1	n_1	E_1	log k_2	E_2	log k_3	n_3	E_3
	mol/m^2/s	–	kJ/mol	mol/m^2/s	kJ/mol	mol/m^2/s	–	kJ/mol
Quartz	–	–	–	−13.34	90.10	–	–	–
K-feldspar	−10.06	0.50	51.70	−12.41	38.00	−21.20	−0.82	94.10
Albite	−10.16	0.46	65.00	−12.56	69.80	−15.60	−0.57	71.00
Anorthite	−3.50	1.41	16.60	−9.12	17.80	–	–	–
Annite	−9.84	0.53	22.00	−12.55	22.00	–	–	–

[1]Chemical affinity parameters p and q default to unity if not specified
[2]log k computed at 25 °C and pH = 0

11.2.3 OGS-IPQC Solution

The fracture is meshed into 60 line elements with a length of 1 mm. The initial concentrations, pH value and pe value at each element are 0 mol/m^3, 7.0 and 4.0, respectively. Dirichlet-type boundary conditions are set at the inlet. Element concentrations are assigned as 0 mol/m^3. PH value and pe value are assigned as 7.0 and 4.0, respectively. Hydraulic pressure is prescribed as 0.04 MPa. The .pqc file is responsible for preparing the input file for Phreeqc. The automatically-generated phinp.dat file sends the solution composition calculated at the last time step and configurations of mineral dissolution/precipitation rates to the Phreeqc for batch-reaction calculations. It is noteworthy that the water volume in a discretized fracture element is 1.70763×10^{-7} kg.

11.2.4 Phreeqc Solution

Time step is a key parameter in the transport module in Phreeqc which is used to control the fluid velocity. Before activating kinetic reactions, some tracers are put into the water at the inlet and the arrival time at the outlet is recorded. By this way, we can calculate the fluid velocity in the fracture and make sure it has a same value in the OGS#IPQC simulator.

11.2.5 Results

The evolution of element concentrations (K, Si, Fe, Mg, Na, Al and Ca) and pH value at the outlet simulated by Phreeqc and OGS#IPhreeqc are illustrated in Fig. 11.5. Element concentrations and the pH value are in a good agreement. Before the water

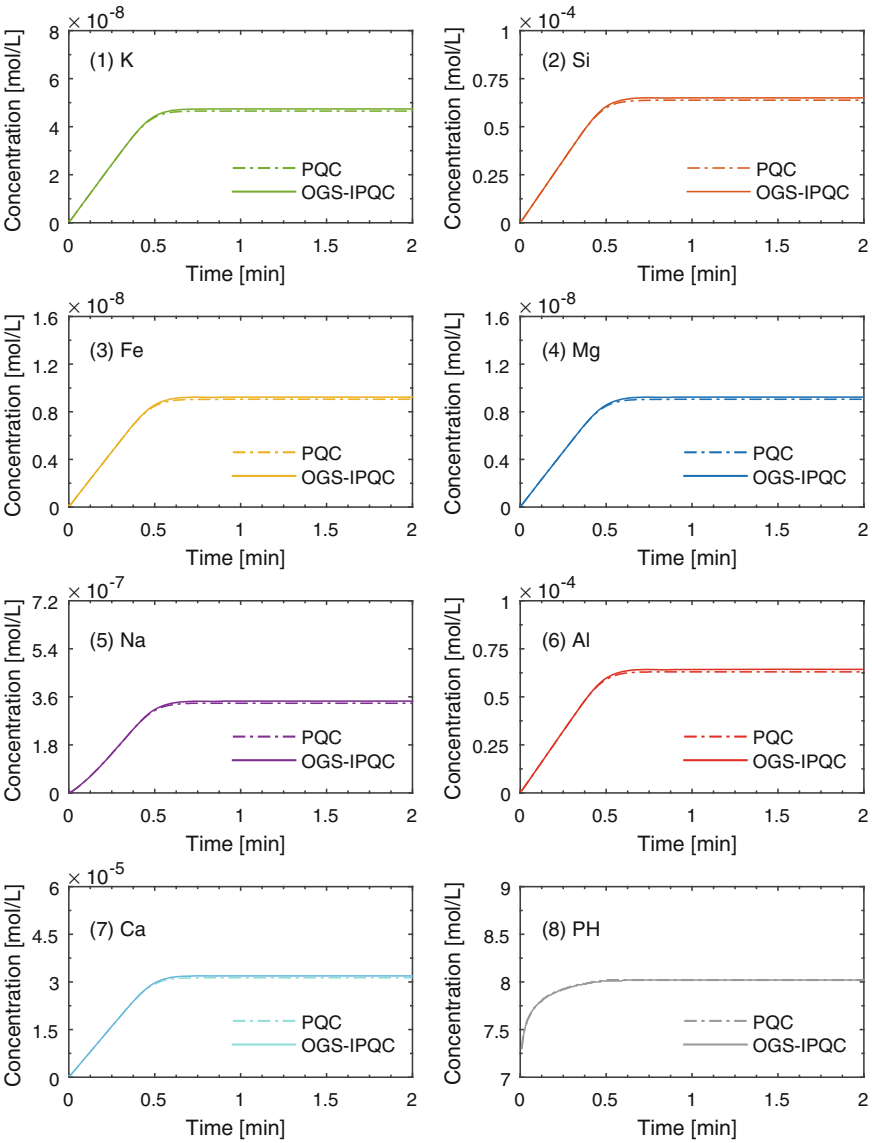

Fig. 11.5 Evolution of element concentrations (K, Si, Fe, Mg, Na, Al and Ca) and pH value at the outlet

front arrives at the outlet, element concentrations grow linearly due to continuous mineral dissolution. After that, the new-formed aqueous species will be taken away with the flowing water.

Acknowledgments The authors appreciate and thank the Funding Organisations for their financial and technical support of the DECOVALEX project work described in this paper. The statements made in the paper are, however, solely those of the authors and do not necessarily reflect those of the Funding Organisation(s). Also, no responsibility is assumed by the authors for any damage to property or persons as a result of operation or use of this publication and/or the information contained herein.